Improved classification of Alzheimer's disease and mild cognitive impairment through dynamic functional network analysis

Nicolás Rubido[1$], Venia Batziou[2$], Marwan Fuad[2], Gernot Riedel[3], and Vesna Vuksanović[2,*]

[1]University of Aberdeen, Aberdeen Biomedical Imaging Centre, AB25 2ZG, United Kingdom
[2]Swansea University Medical School, Swansea University, SA2 8PP Swansea, United Kingdom
[3]Institute of Medical Sciences, University of Aberdeen, AB25 2ZG, United Kingdom
[*]Correspondence: vesna.vuksanovic@swansea.ac.uk
[$]These authors contributed equally

ABSTRACT

Brain network analysis using functional MRI has advanced our understanding of cortical activity and its changes in neurodegenerative disorders that undelie dementia. Recently, research in brain connectivity has focused on dynamic (time-varying) brain networks that capture both spatial and temporal information on cortical, regional co-activity patterns. However, this approach has been largely unexplored within the Alzheimer's spectrum. We analysed age- and sex-matched static and dynamic fMRI brain networks from 315 individuals with Alzheimer's Disease (AD), Mild Cognitive Impairment (MCI), and cognitively-normal Healthy Elderly (HE), using data from the ADNI-3 protocol. We examined both similarities and differences between these groups, employing the Juelich brain atlas for network nodes, sliding-window correlations for time-varying network links, and non-parametric statistics to assess between-group differences at the link or the node centrality level. While the HE and MCI groups show similar static and dynamic networks at the link level, significant differences emerge compared to AD participants. We found stable (stationary) differences in patterns of functional connections between the white matter regions and the parietal lobe's, and somatosensory cortices, while metastable (temporal) networks' differences were consistently found between the amygdala and hippocampal formation. In addition, our node centrality analysis showed that the white matter connectivity patterns are local in nature. Our results highlight shared and unique functional connectivity patterns in both stationary and dynamic functional networks, emphasising the need to include dynamic information in brain network analysis in studies of Alzheimer's spectrum. Furthermore, we trained a Random Forest model on the extracted dynamic network features, which provided robust classification performance in distinguishing MCI, AD, and HE groups, demonstrating the diagnostic potential of time-varying connectivity metrics.

Introduction

Brain networks derived from functional magnetic resonance imaging (fMRI) have improved our understanding of cortical functional connectivity, i.e., patterns of co-activity between remote cortical processes[1–3]. Mapping functional networks from neuroimaging data, has been useful in providing information about altered cortical activity in brain disorders[4–7]. In Alzheimer's disease (AD), functional networks differ from the patterns of connectivity observed in healthy individuals[8–12], and the magnitude of these differences often correlates with the underlying abnormal accumulation of missfolded tau protein and deposits of amyloid-beta, or white matter damage[13]. Differences also correlate with the severity of clinical symptoms, assessed using cognitive and behavioral metrics[14–18]. Network-based studies further demonstrate that while brain disorders like AD exert a global effect on the brain, their impact is heterogeneous, with certain regions, particularly the central (hub) areas of the temporal, parietal, and frontal regions associated with higher-order cognitive functions, being more severely affected[19,20].

Alzheimer's disease is increasingly recognised as a disconnection syndrome, disrupting brain networks and leading to cognitive and behavioral decline[21]. Network changes are observed in Mild Cognitive Impairment (MCI)[22,23], a cognitive disorder that may progress to AD. However, the impact of MCI and AD is not always proportional to their cognitive severity. Both, MCI and AD, impact local[24,25] and small-world network metrics[26,27] through changes in clustering (i.e., segregation)[28] and global efficiency (i.e., integration)[29–31]. Betweenness centrality[32,33], modular organization[34–36] and reduced functional connectivity within the default mode network[37–40], have also been consistent findings throughout studies.

Recently, dynamic brain network analysis, which considers temporal fluctuations in the resting-state fMRI signal, has revealed patterns of activity that are usually averaged out by conventional functional network analysis. These patterns of

activity, termed dynamic functional networks (dFNs), reveal transient (metastable) dynamical states, whose flexible links (reconfiguration) support cognitive processing[41,42]. Analysis of dynamic functional networks from functional brain recordings, i.e., those acquired over a period of time, has shown the potential to reveal clinically relevant information[43,44]. For example,[45] demonstrated decreased flexibility of interactions in peripheral regions of the language network in patients with temporal lobe epilepsy, due to reduced metastability, which was associated with decreased verbal fluency. Recent studies on dFC in schizophrenia have shown different dwell times in two states, particularly along FC within the default mode (DMN) and language networks[46,47]. These findings highlight the importance of integrating temporal information into brain network analysis. However, in addition to a few recent studies[48–52], this approach remains largely unexplored in the context of functional network disruptions in the Alzheimer's spectrum. In addition, comparative analyses of static and dynamic FNs in AD are lacking.

In this study, our aim was to investigate the potential of fMRI-derived cortical functional networks to assess disrupted connectivity in AD. Using comparative analysis of dynamic and static functional networks, we studied whether the temporal characteristics of functional connectivity are more effective than static ones in identifying reliable functional networks' features in individuals with AD compared to normal ageing and MCI. In addition, we examined sensitivity and specificity of these features to identify AD and MCI individuals from healthy elderly. We hypothesised that dFNs in AD behave differently compared to HC and MCI, reflecting disrupted functional connectivity patterns associated with AD.

Results

Static and Dynamic Functional Networks: the Link Level Analysis

Figure 1 shows statistically significant ($p \leq 0.05$) links across static functional networks (sFNs) based on the Kruskal-Walis (K-W) test, where the links correspond realization-averaged p-values obtained from 100 K-W tests. Each test was performed on 50 randomly sampled single-subject networks in each cohort (realizations) for the (i, j)-the node pair. There were 183

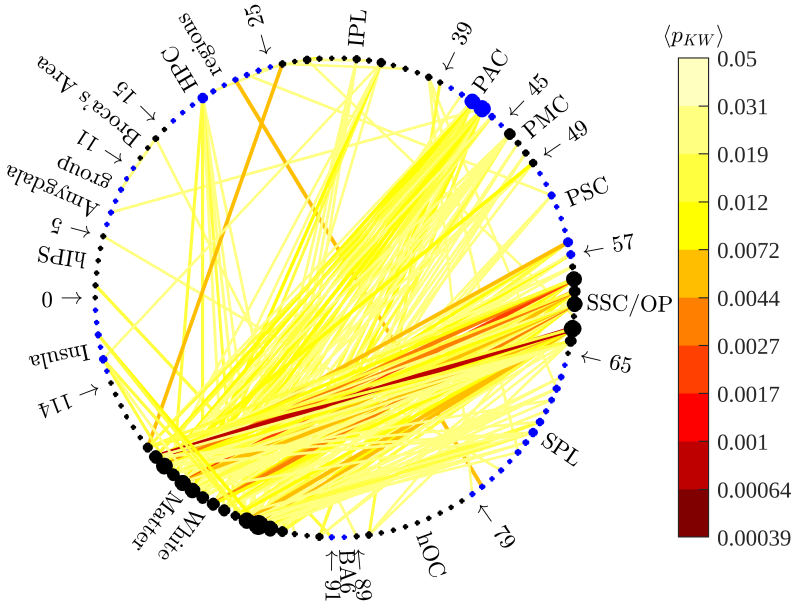

Figure 1. Static functional network differences at the link level across the three study groups. Links (i.e., pairwise correlations) are shown between nodes of the Juelich Brain Atlas arranged on a circle when they pass the Kruskal–Wallis test applied to each link's bootstrapped distribution. P-values are colour-coded.

significant p-values that survived the tests, revealing differences at the link level for sFNs between the groups, which mainly map the functional connections between white matter (WM) and the parietal, frontal, and temporal lobes' regions. The parietal lobe shows significant differences in the static correlations of the Inferior and Superior parietal Lobules (IPL and SPL) and Primary and Secondary Somatosensory Cortices (PSC and SSC/Operculum parietal), where the most prevalent and significant differences appear in the connections between the SSC/OP to WM regions. The links connecting the frontal lobe and WM regions, show the differences predominantly in the primary motor cortex (PMC), whereas the links from the temporal lobe to WM regions show differences predominantly mainly in the primary auditory cortex (PAC) and the hippocampus formation (HPC).

Figure 1 also represents a reference for inter-cohort analysis of static and dynamic functional networks (dFN), and the post-hoc, pairwise comparisons between the HC, MCI, and AD cohorts. In addition, using the K-W tests on the realisation-averaged p-values for dFNs (as shown in Fig. 2), can help to determine which dynamic correlation exhibit stationary characteristics and which demonstrate transient meta-stability across the cohorts. Specifically, significant p-values identified in the K-W tests for dFNs are considered static if they also appear in the K-W test for sFNs; otherwise, they are classified as transient, revealed through the sliding window analysis.

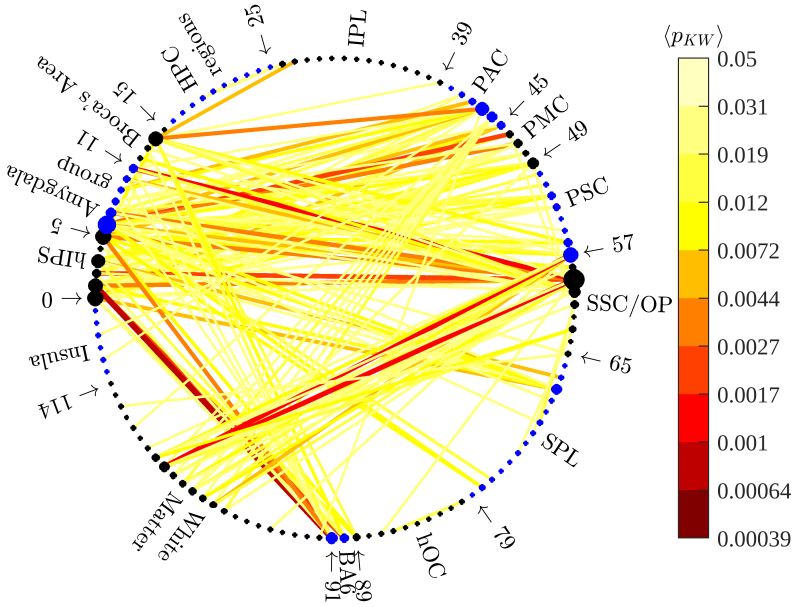

Figure 2. Dynamic functional network differences at the link level within the three study groups. Links (i.e., pair-wise correlations) are shown between nodes of the Juelich Brain Atlas arranged on the circle when they passed the Kruskal-Walis tests applied to the each link's bootstrapped distributions. Dynamic functional connectivity was estimated using sliding windows of 60s in length. P-values are colour-coded.

Statistically different dynamic functional links are shown in Fig. 2. There were 148 links whose p-values $\langle p_{KW}(i,j;t_0 = 90, \Delta t = 20)\rangle \leq 0.05$ survived the K-W test of differences within the study group. The links highlights patterns similar to those in Fig. 1. Although the strength in the connections from the WM regions to SSC/OP and PAC appears different from that in Fig. 1, the appearance of the links in Fig. 1 implies a stationary nature of these connections. Functional connections mapped using dFN analysis that are missing in Fig. 1, were found between Broca's Area, the Amygdala group, and the anterior Intra-parietal Sulcus (hIPs) with the SSC/OP, PSC, PMC, PAC, and Premotor Cortex (BA6), revealing temporal (meta-stable) nature of these connectivity patterns.

In addition to dFNs analysis of differences within the study groups, we also show the frequency of significantly different tests (links) across sliding windows (i.e., how many times the distribution of correlations between a (i,j) cortical pair was statistically different as the window used for dFN analysis slides along the fMRI time series). The frequency ranges from 12 to 4 appearances, out of the maximum of 18 sliding windows – see Fig. 3.

Pair-wise analysis of the static networks between groups: the link level

Post-hoc pair-wise comparisons of sFNS links were performed between AD/HC, AD/MCI and MCI/HC groups following the K-W test. There were 279 significantly different links for AD/HC [Fig. 4 (left)] and 150 significantly different links for MCI/HC [Fig. 4 (right)]. For the AD/MCI comparisons, there were 150 links that survived significance tests at the ($<$0.05) level and there were no significant links for the increased $p < 0.01$ level.

Fig. 4 (left panel) shows statistically different functional connections which involve the WM regions connected to multiple gray matter (GM) regions predominantly in the parietal, temporal and frontal lobes. The GM regions are: the Primary Auditory Cortex (PAC), Primary Motor Cortex (PMC), Primary Somato-sensory Cortex (PSC), Secondary Somato-sensory Cortex (SSC), and Superior parietal Lobule (SPL) regions. On the other hand, Fig. 4 (right panel) shows that the MCI/HC differences map out predominantly patterns of connections within GM. The connections include: the hippocampus formation (HPC) and the pre-motor cortex (BA6), the SPL with the Insula, and the PSC with the Inferior parietal Lobule (IPC) and HPC. Significantly different AD/MCI links (at p$<$ 0.05) are between WM and GM regions – the SSC regions and Insula.

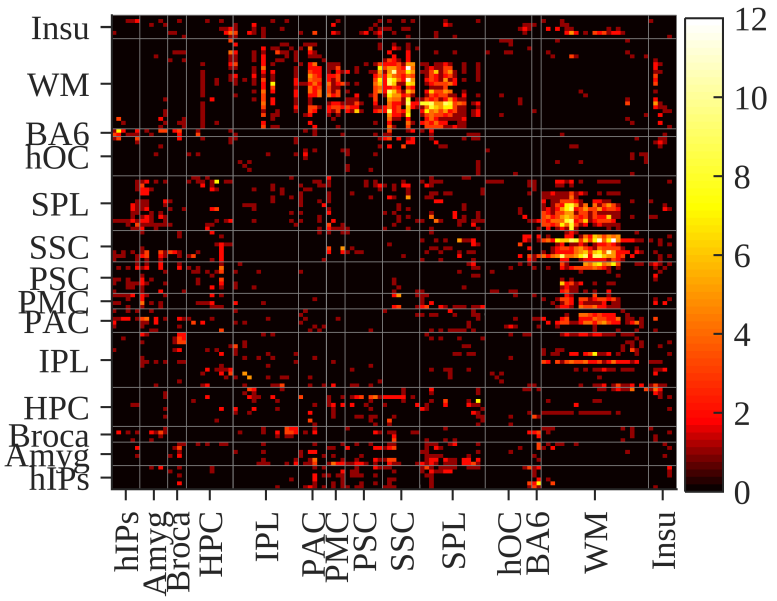

Figure 3. Number of significant realisation-averaged p-values in the sliding-window analysis. Number of times each realisation-averaged p-value is significant in all 18 sliding windows for each pair of Juelich Brain Atlas regions.

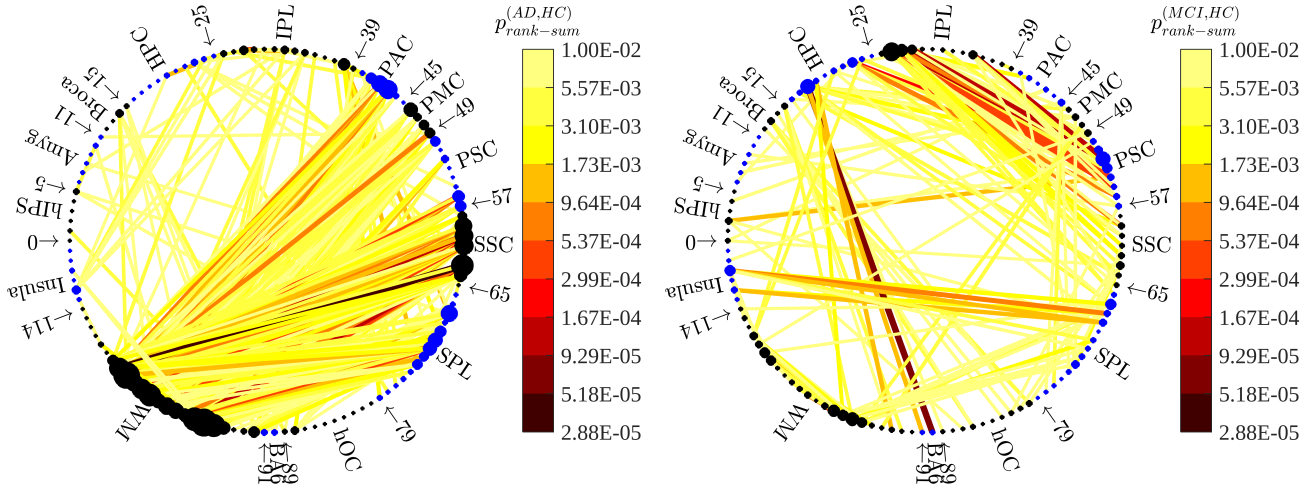

Figure 4. Significant differences at the link level between groups. Links (i.e., pair-wise correlations) are shown between nodes of the Juelich Brain Atlas arranged on the circle when they passed the Kruskal-Walis tests applied to the each link's bootstrapped distributions (100 values for each test). P-values are colour-coded. Abbreviations: Alzheimer's disease (AD), mild cognitive impairment (MCI) and healthy controls (HC).

To establish confidence intervals for the pairwise between-group differences, we repeated the corresponding statistical tests on resampled (bootstrapped) cohorts. Specifically, we generated 100 bootstrap samples for each group by randomly selecting ($N = 50$) participants (i.e., 50 from each group, matched by the corresponding male/female ratio between the groups). The results of this, more stringent statistical analysis, showed similar results: Most of the 248 links for HC/AD survived, and were found between the same WM and GM regions that also appear in Fig. 4 (left panel). Similarly, the 158 survived links for the AC/MCI comparisons were found between GM region highlighted in Fig. 4 (left panel). However, there were only 7 significantly different links for HC/MCI, and none of the tests survived multiple comparisons corrections of the p-values, which indicates that a larger cohort potentially corroborate these results.

The static networks of the resampled groups at the link level: deviation from healthy controls

To investigate the deviation of functional correlations patterns in sFNs from healthy controls, (i.e., whether there is an increase or decrease in these correlations from HC), we visualised patterns of these changes in respect to the median sFN of the HC group. In Fig. 5 each cohort's median correlation for a pair of nodes were colour coded to illustrate the strength of the correlations. For example, the median value of the links between the SSC and WM regions for HC cohort is $\simeq 0$, meaning nearly uncorrelated functional activity between these regions. However, these became positive in AD, where we observed correlation values $\simeq 0.25$. Similarly, links between the PMC and WM have negative median values in HC $\simeq -0.25$, but became uncorrelated (i.e., $\simeq 0$) in AD. Similar patterns of these deviations from HC, can be seen in MCI [Fig. 5 (right panel)], however, the magnitude of these deviations is smaller. Please see also Section , where we show that there are 150 significant p-values between MCI and HC cohorts, but nearly as many as 279 between AD and HC cohorts.

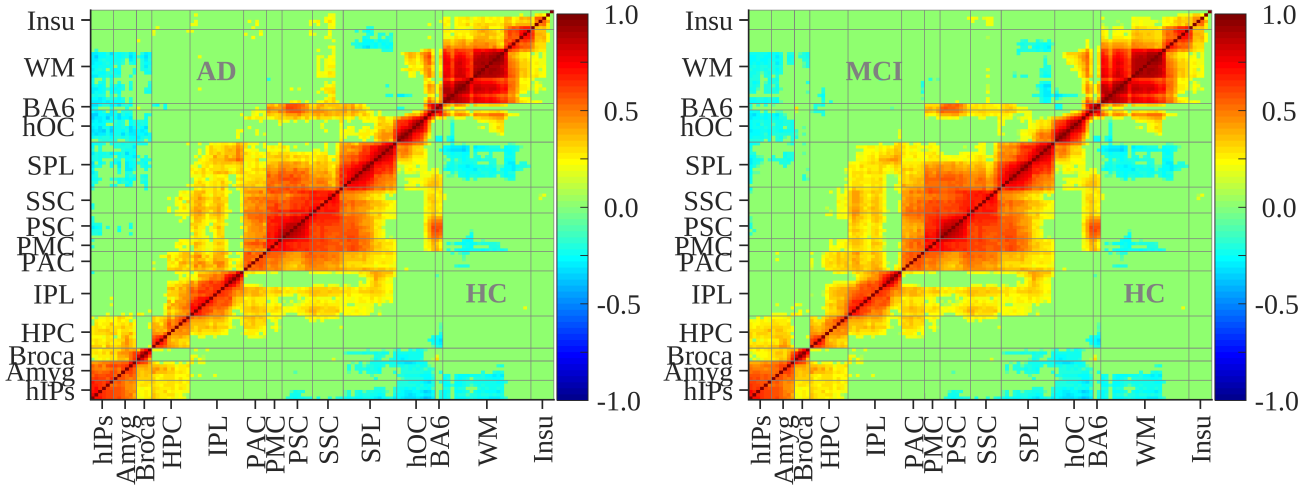

Figure 5. Cohorts' median static correlations. Upper diagonal entries show the median static correlation values (color-coded) for the AD/MCI cohort, and lower diagonal entries show the corresponding values for the HC cohort. Abbreviations: Alzheimer's disease (AD), mild cognitive impairment (MCI) and healthy controls (HC).

When comparing the sFNs between AD and MCI cohorts (data not shown), we saw similar patterns: higher correlations in ADs than in MCIs and 195 significant p-values for pair-wise correlations. Some interesting observations are: the WM and the SSC sFNs are close to zero for the MCI cohort – the same as for the HC cohort in the lower diagonal entries of Fig. 5. In addition, the links between the WM regions and the Insula were significantly different only between AD ($r \simeq 0.50$) and MCI ($r \simeq 0.25$) cohorts, but there were no differences between HC and AD.

Inter-cohorts differences in dynamic functional networks: the link level

Fig. 6 shows dFN links' frequency count for between-cohorts differences, by sumarising a significant inter-cohort difference across the sliding windows (similar to Fig. 3 for within-cohort differences), where Fig. 6 (left) is for AD/HC and Fig. 6 (right) for MCI/HC.

Consistent with our analysis, most of the inter-cohort differences are driven by the connections of the WM with the SSC and the SSL regions for AD/HC, where there is the maximum of 14 appearances [found between the intra-hemispheric connection between nodes 63 (right secondary somatosensory cortex) and 107 (right optic radiation)] for AD/HC. High frequency was also found between WM and SPL regions, and between WM and PSC, PMC, and PAC regions. The right panel of Fig. 6 shows that the dFNs links' frequency between MCI and HC participants is high within the WM regions, where the inter-hemispheric connection between regions 100 and 101 (inferior occipito-frontal fascicle l/r) was different across 12 sliding windows.

For AD/MCI differences (data not shown), we found that the functional connection between between nodes 63 and 107 was significant across 12 sliding windows, which is the same result as for AD/HC. However, some GM to GM connections were different from those in AD/HC. For example, differences in the links between the IPL with Broca's Area and the PAC with Amygdala, which were not found in MCI/HC or AD/HC.

Fig. 6 (left panel) shows that the frequency of significant links in dFNs for AD/HC follows the pattern similar to the sFNs analysis [see Fig. 3]. However, this is not the case for MCI/HC, where the dFNS analysis [see Fig. 6 (right panel)] highlights changes within the WM networks, whilst the sFNs analysis, [see Fig. 4], highlights connections within the GM networks.

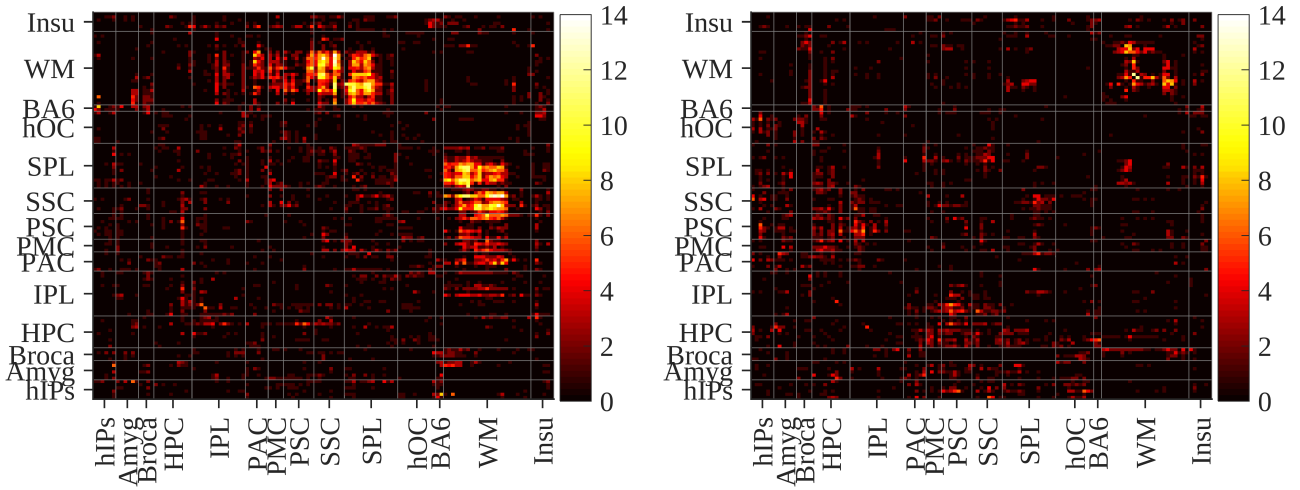

Figure 6. Inter-cohorts differences between static and dynamic functional networks (s/dFN) at the link level. Colour code represents the number of times a dFN link differ from a sFN link between AD/HC (left panel) and MCI/HC (right panel). Abbreviations: Alzheimer's disease (AD), mild cognitive impairment (MCI) and healthy controls (HC), static/dynamic Functional Connectivity (s/dFC).

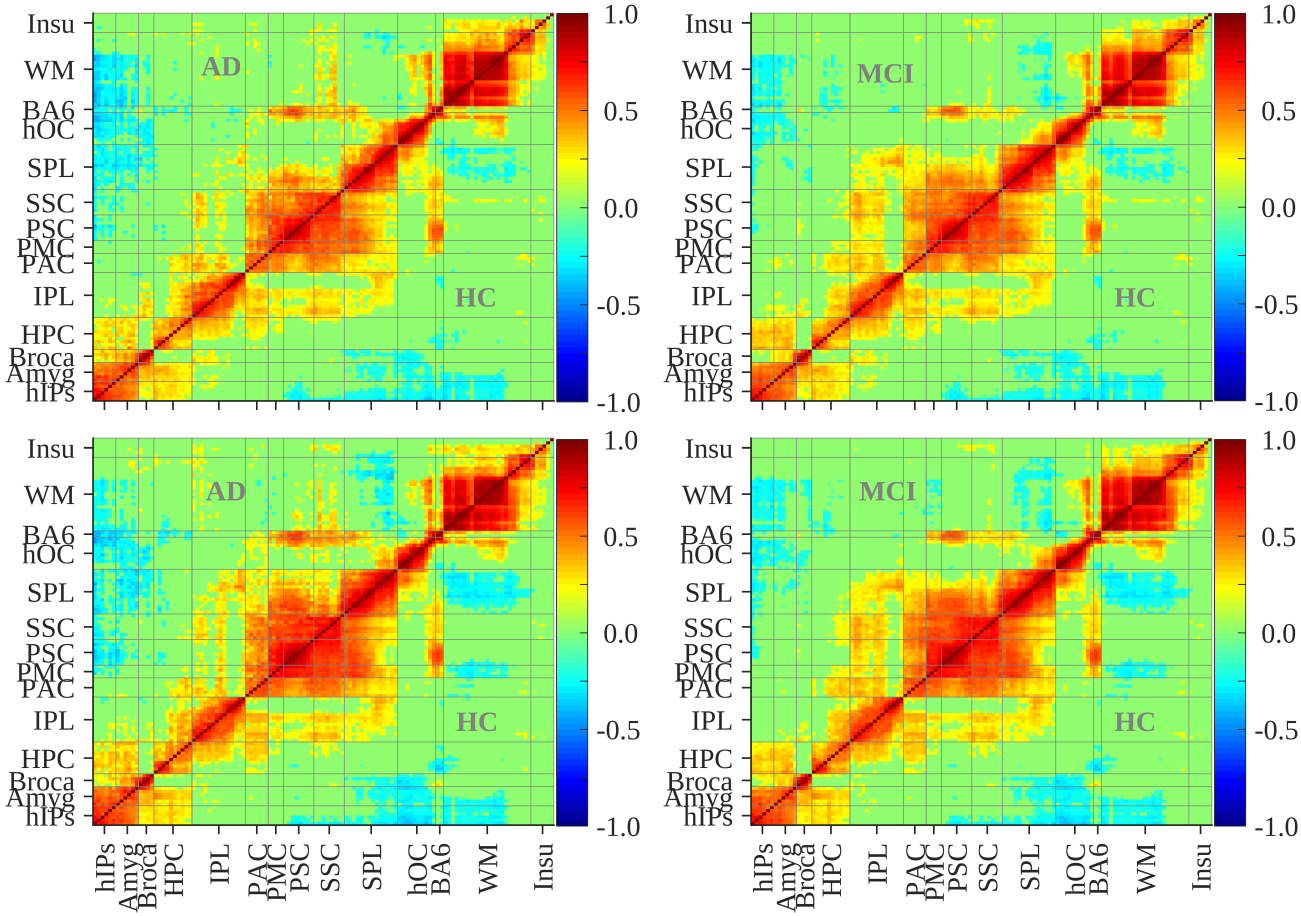

Figure 7. Cohorts' median sliding-window correlations. Left panels: median values for AD (upper diagonal elements) and HC (lower diagonal elements) cohorts of the correlations. Right panels: median values for MCI (upper diagonal elements) and HC (lower diagonal elements) cohorts. Only data for first (top) and last (bottom) sliding windows are shown. Abbreviations: Alzheimer's disease (AD), mild cognitive impairment (MCI) and healthy controls (HC).

The dynamic networks on the resampled groups at the link level: changes from healthy controls

Similarly to the analysis for sFNs (showed in Fig. 5), we visualised deviation of dFNs links with respect to the HC group. In terms of the direction of the deviation, the results were less consistent than those in the sFNs. That is, some of the correlations increase and other decrease (see Fig. 7), which indicates that non-stationary variations in the functional connections are missed in static analysis.

For example, we saw that the functional connections between the SPL and WM regions for the HC cohort that have negative median correlation values $\simeq -0.25$) (top panels in Fig. 7), while these connections were still present in MCI cohort they disappear in AD $\simeq 0$ (see top left panel of Fig. 7]. Similarly, the IPL and SSC regions regions were not connected with the WM regions in HC or MCI ($\simeq 0$), but in AD the connections between them were positive $\simeq 0.25$), which is similar behaviour to that observed for the sFNs. However, differences appear between IPL and SPL connections in the first window [Fig. 7 (upper panels)] in HC and AD, while this deviation was not observed in MCI. Similarly, the PSC and SSC regions were not connected to the WM region in HC and MCI [Fig. 7 (lower panels)], but they were positively correlated in AD. Another notable non-stationary deviation is in the PSC and the Amygdala group links, which were $\simeq 0$ in HC and MCI, but negative in AD $\simeq -0.3$.

Dynamic and Static Functional Networks: Node Strength and Eigenvector Centrality

Fig. 8 shows analysis of two measures of network centrality – node strength and eigenvector centrality – between sFN (top panels) and dFNs (bottom panels) within the three groups. Visually, there are only a few differences between sFN and dFN centrality measures. Most of the significant differences in node strength, for both sFN and dFN, were found between the WM regions (grey bands and asterisk in the plots), where some differences overlap between the two networks (s/d). We interpret the non-overlapping dFN nodes that become stationary in sFNs as those with the metastable dynamic. These nodes are the HCP, IPL and Insula.

Eigenvector centrality shows similar behaviour of both, the sFNs and dFNs [Fig. 8 (right panels)] however, only the sFN reached significant differences for four nodes (Amygdala, HPC, SPL and hOC). The most striking result is lack of significant differences within the WM regions, which was almost a constant in all other analysis. We suggest that all differences in the WM regions are local in nature and that they disappear when looking at the centrality measure which takes into account global connectivity.

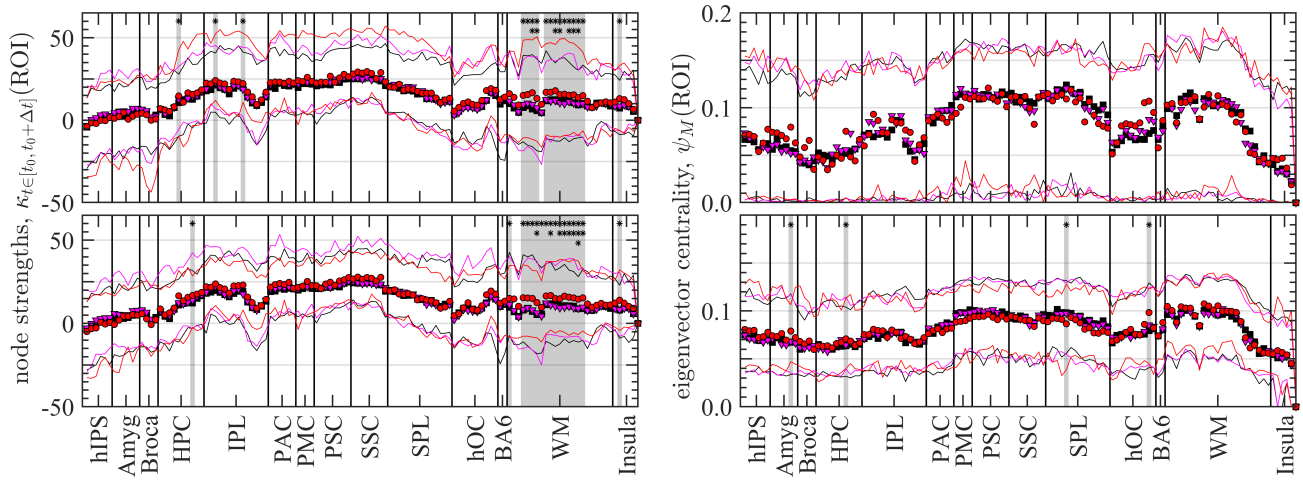

Figure 8. Weighted node centrality measures for static and dynamic functional brain networks. Left panels: node strength of the Jülich Brain Atlas, where vertical lines reference the ROI endings and shaded areas highlight significantly different medians between HC and AD cohorts ($*$: $0.001 < p \leq 0.01$, $**$: $10^{-4} < p \leq 0.001$, and $***$: $p \leq 10^{-4}$). Top [Bottom] panels: centrality values for the static [dynamic] correlations that use all the BOLD signal [use sliding windows with $t_0 = m\Delta t/2$, $\Delta t = 20$, and $m = 0, 1, \ldots, 17$]. The centrality values for the dFN of each participant (bottom panels) are here averaged over the 18 sliding windows. Filled symbols represent the cohort's median value for each ROI and continuous lines the interval containing 95% of the cohort's centrality values. The median values for HC are shown by black squares, for MCI by purple triangles, and for AD by red circles, with their respective 95% lines in the same colours. Abbreviations: Alzheimer's disease (AD), mild cognitive impairment (MCI) and healthy controls (HC).

Random Forest Classification

Table 1 shows the results of the random forest (RF) models trained on BOLD time series data. We classified the time series using three different classes of inputs: (i) set of nodes from 7 to 26, i.e., nodes of the amygdala and hippocampal formation, which were found to be relevant for metastable (temporal) networks, (ii) set of WM nodes (92 to 114), significantly different in terms of stable (stationary) patterns, and (iii) a subset of nodes in WM – nodes 95 to 112 – that were found to be different in terms of local and global network metrics. The classifier was used on the whole time series of 197 points and windows of Δt = 20, 40 and 60s. In general, the RF classifiers performed better when only two groups were pooled together, achieving the highest accuracy of $\approx$ 76% between HC and AD groups for the first set of nodes (of the amygdala and hippocampus formation) and also for the third set of nodes (WM nodes 95 to 112) for Δt = 60s. Across all configurations, the highest accuracies were consistently achieved with a window size of Δt = 60s, including an accuracy of approximately 74% – the best result for three-group classification – and a significant improvement over previous results[53].

		Accuracy (%)			
Nodes	**Groups**	T= 197	Δt = 20	Δt= 40	Δt = 60
7 – 26	MCI vs AD	50.6±3.1	52.8±1.7	53.0±4.1	58.8±3.1
	MCI vs AD	73.6±.8	73.6±.8	73.1±1.2	73.6±1.1
	HC vs AD	75.5±.7	75.4±.7	75.4±.7	79.4±1.4
	HC + MCI + AD	46.4±2.2	45.4±3.2	44.8±3.0	57.8±2.5
92 – 114	MCI vs AD	73.6±.8	73.6±.8	73.6±.8	74.2±1.1
	MCI vs HC	52.6±.3	53.1±1.7	53.2±2.1	71.8±2.0
	HC vs AD	75.4±.7	75.4±.7	75.4±.7	78.7±1.2
	HC + MCI + AD	45.8±2.6	47.6±2.1	50.0±1.5	63.0±2.5
95, 96, 100:108,111, 112	HC vs AD	75.5±0.8	75.5±0.8	75.5±0.8	76.5±1.1
	HC vs MCI	55.5±2.1	49.1±2.1	53.2±2.4	68.5±2
	AD vs MCI	45.4±3	50.2±3.1	42.5±2.5	67.5±2
	HC vs (AD + MCI)	54.0±2.0	47.6±2.0	52.7±2.6	74.3±3.2

Table 1. The accuracy of the Random Forest classifier on the entire time series of 197 time points and on windows of Δt = 20, 40 and 60 points, reported as the mean $\pm$ standard error. The classifier was trained using 10-Fold Cross-Validation based on 100 decisions trees. For the nodes names see the SI Table 1.

Discussion

In this study, we conducted static and dynamic analyses of cortical functional networks, derived from fMRI data, in a cohort of 315 individuals from three, age- and sex-matched, clinical groups: Alzheimer's disease, mild cognitive impairment, and healthy older adults. Our analyses suggest that combining information from static and dynamic functional networks offers a more complete picture of brain connectivity and its changes in people with dementia and cognitive impairment.

Our comparative analysis of sFNs and dFNs highlighted distinct drivers of local and global functional connectivity patterns between groups. For example, while white matter regions displayed consistent connectivity differences across groups, these differences were not evident in nodal centrality measures that drive global (network) connectivity. In addition, static functional networks revealed significant differences in connectivity at the link level across the three groups, particularly in connections between white matter and the somatosensory, primary auditory, and hippocampal cortices. This contrasts dynamic functional networks (dFNs), whose transient connectivity changes and meta-stable states, which are not detectable with static analysis, revealed differences in connectivity between the amygdala and inferior parietal and prefrontal cortex and hippocampal formation between AD and MCI individuals.

Studies have suggested that dFNs can reveal clinically relevant information by highlighting variations in connectivity that occur over shorter time scales[48,54]. For example, dFNs have been a better predictor of cognitive impairment in AD, compared to conventional static FNs (see, e.g.,[55]), and have improved distinction of AD from MCI or HC subjects[50,55]. It has been suggested that these improvements are based on the dFNs ability to better capture the flexibility and adaptability of functional networks to reconfigure on cognitive demands[56,57]. Some of our results that are worth dusscusing in the context of dFN characteristics as biomarker of differences between AD and MCI are: (i) consistent inter-cohort differences driven by the connectivity pattens between the WM regions and somatosensory cortices, (ii) appearance of (temporal) links between the Broca area and amygdala with the hippocampal formation and (iii) strikingly similar results for network centrality metrics between sFN and dFN revealing that the WM functional connections are local in nature.

The most consistent results are the inter-cohort differences that are driven by the connectivity patterns between the WM regions and somatosensory cortices (Figs. 1,2,3,4 and 6). This is an interesting finding, as it is generally thought that AD spares primary sensory function. However, recent findings suggest that such interpretations have been drawn from a literature that has rarely taken into account variability in cognitive decline seen in AD patients[58]. Cognitive domains affected by AD, are now known to modulate cortical somatosensory processing; that is, it is possible that abnormalities in somatosensory function in patients with AD have been suppressed by neuropsychological variability not accounted for in previous research. Supporting this hypothesis are recent studies that have revealed a dynamic interplay between somatosensory neural systems and the pre-frontal cortex that support attention and executive functions[59]. Patients with AD often have impaired attention and executive functions, but these impairments are highly variable between individuals, and it is possible that controlling for variability in these cognitive domains would reveal differences in somatosensory processing in these patients, as suggested by[58]. Our findings suggest that dFN could be used as a biomarker of decline in AD, which is independent of their (subjective) cognitive scores.

Another interesting finding is the appearance of (temporal) links between the Broca area and the amygdala with the hippocampal formation (Fig. 2). The importance of the amygdala-hippocampal connections and their role in AD has been well documented (for review, see[60]). For example, impaired amygdala-hippocampus connectivity in AD is associated with impaired cognitive functions such as episodic and emotional memory, working memory formation, and anxiety and depression. It is also associated with patho-physiological abnormalities in tau protein hyperphosphorylation, impaired insulin signaling, $A\beta$ plaque formation, synaptic failure, and imbalanced cholinergic neuron innervation[60]. Again, dFN analysis was able to identify these 'hidden' patterns of activity in AD patients, which were concealed by longer, stationary brain processes.

Finally, our comparative analysis has revealed that the variability in eigenvector centrality, which has been identified as "an early biomarker of the interplay between early Alzheimer's disease pathology and cognitive decline" in healthy individuals[61], is driven by temporal FNs identified through the link level analysis. Lorenzini et al., demonstrate that changes in EC, as well as EC variability over time, are involved in the neurofunctional manifestation of the early stages of Alzheimer's disease. Here, we provide evidence that EC differences were driven by the amygdala-hippocampus formation connectivity, which has been identified as an indicator of abnormal brain function in early AD[62].

In this study, we used dFNs to investigate temporal fluctuations and transient (meta-stable) patterns of brain activity, in age- and sex-matched AD, MCI and healthy elderly individuals. In a comparative analysis study between sFN and dFN, we provided evidence for similarity and differences between the two methods. We found consistent inter-cohort differences driven by the connectivity pattens between the WM regions and somatosensory cortices, indicating their stationary nature. dFNs revealed temporal characteristics of the links between the amygdala and the hippocampal formation, associated with neuropathological as well as cognitive hallmarks of AD. Explanation of the differences in variations of centrality metrics between sFN and dFN, revealed that the WM links are local in nature.

Methods

Participants and Cohorts

Data used in this study were obtained from the Alzheimer's Disease Neuroimaging Initiative (ADNI) data base. We downloaded demographic, clinical and MRI data from $N = 315$ individuals participating in the study. The main inclusion criterion was that the fMRI datasets were acquired using the same resting-state protocols (see the Imaging Datasets Section for details). The 315 participants were selected from three groups: Healthy Controls (HC), Mild cognitive Impairment (MCI), and Alzheimer's Disease (AD) groups. Demographic and clinical characteristics of the participant averaged across each group were shown in Table 2.

Demographics	**HC**	**MCI**	**AD**
Number of participants	141	128	46
Age (s.d.)	79.52 (5.60)	76.77 (4.72)*	78.46 (5.91)
Sex (F:M)	68 : 73	52 : 76	17 : 29
Clinical Scores			
MMSE (s.d.)	28.19 (3.64)	27.57 (2.47)	22.39 (3.84)*,**

Table 2. Participants' demographic and clinical characteristics. Abbreviations: M-male, F-Female, s.d.-standard deviation, HC-healthy controls, AD-Alzheimer's Disease, MCI-Mild Cognitive Impairment, * significant difference ($p < 0.01$) from HC. ** significant difference (i.e., $p < 0.01$) from MCI.

Imaging Datasets and Processing

We analysed resting-state functional (rs-fMRI) images from 315 participants. fMRI were acquired using ADNI-3's basic EPI-BOLD protocol (details at ADNI's website) and in[63]. In short, the scanning time of each participants was for up to 10 minutes using the same two-time accelerated 3 T scanner, following an even/odd interleaved axial-slicing (inferior to superior) of 3.4 mm with $(3.4375\,mm)^2$ pixels (FOV = 220×220; $P >> A$ phase encoding; TE = 30 ms; TR = 3 s).

Image preprocessing, which includes brain extraction, registration in standard MNI space, and brain tissue segmentation was carried out using FMRIB's pipeline *fsl_anat* in its default settings. Pre-processing of fMRI is done by applying FMRIB's Expert Analysis Tool, *FEAT*, resulting in Blood-Oxygen-Level-Dependent (BOLD) signals of $N_T = 197$ data points ($197\times$ TR acquisition times) for each voxel. Please see the Supplementary Information for a more detailed description of the image processing and the steps applied.

Networks Construction: Static and Dynamic Functional Connectivity

Cortical regions – defining the network nodes – are based on the Jülich brain atlas (JBA)[64], resulting in cortical parcellations 120 regions (details of the atlas in SI). We also preformed analyses on another standard FSL atlas – Harvard-Oxford brain atlas (H-OBA), which parcellates cortex into 48 regions. Our main results are reported for the JBA analys, while the H-OBA results are reported in the SI. The signal of each node is calculated by averaging the rs-fMRI BOLD time series across all voxels within the corresponding region/node.

Functional links were defined by the Pearson correlation coefficient, r[1,2,65], calculated pairwise between all nodes,

$$r^{(s)}_{t\in[t_0,t_0+\Delta t]}(i,j) = \mathrm{cov}\left[x_{t\in[t_0,t_0+\Delta t]}(i)^{(s)}, x_{t\in[t_0,t_0+\Delta t]}(j)^{(s)}\right]/\sigma_i\,\sigma_j, \tag{1}$$

where $\mathrm{cov}\left[x_{t\in[t_0,t_0+\Delta t]}(i)^{(s)}, x_{t\in[t_0,t_0+\Delta t]}(j)^{(s)}\right]$ is the covariance between the time window $[t_0, t_0+\Delta t]$ of the node signals i and j (from t_0 to $t_0+\Delta t$, where $t_0+\Delta t \leq N_T = 197$), σ_i and σ_j are standard deviations of nodes $i$and j, and s is an index identifying participants from the cohorts. We also set a $p < 0.01$ significance threshold for the value $r^{(s)}_{t\in[t_0,t_0+\Delta t]}(i,j)$ (see Eq. (1), which discards spurious correlations. This definition of functional links results in a single subject, symmetric (undirected), weighted (with positive and negative weights), functional network, containing only statistically significant connections due to the removal of spurious correlations.

To construct links of static functional network, we utilise node signals in Eq. (1) (i.e., $[t_0, t_0+\Delta t] = [0, N_T]$); that is all 197 points of the BOLD singal of a node[1,2,18,23,27,28]. Because of the the $p < 0.05$ significance threshold, which was set in Eq. (1), approximately 39% were discarded from each participant's sFN for the JBA.

To construct dynamic functional network (dFN), we use half-overlapping sliding windows of the node signals as described in[66]. This way, to maintain nominal control of mapping spurious (false positive) correlations within the time windows, the window size was determined by calculating 1/smallest frequency in the data, represented by the high-pass filter cutoff[67]. Specifically, we set $t_0 = m\Delta t/2$ in Eq. (1), with $m = 0, 1, \ldots < N_T/\Delta t$ and $\Delta t = 20$, 40, or 60 data points – accounting for 1, 2, or 3 minutes of scan time, respectively. For a given window size Δt, the functional link $r^{(s)}_{t\in[t_0,t_0+\Delta t]}(i,j)$ changes according to sliding-window time t_0. The significance threshold for the (i,j)-th dynamic link for each participant was set based on the value obtained from its static counterpart: $r^{(s)}_{t\in[0,N_T]}(i,j)$. In this way the thresholds of the sliding-window correlations were set to be either greater or equal from the corresponding static correlations. As a result, for a sliding window of $\Delta t = 20$ points – resulting in 18 half-overlapping windows. The average percentage of discarded links per participant in its dFN was 30% (see Fig. 2). For the H-OBA, the same analysis yielded to about 28% of discarded links.

Functional Networks' Metrics

We characterised functional connectivity in three study groups based on the importance of the network nodes. A straightforward method to assess the importance of a network node is to compute its centrality. The centrality of a node is a measure that quantifies how important or influential a node is within a network. Centrality can be expressed in various ways; thus, there are multiple types of centrality measures. We characterised the importance of each node in the dFNs and sFN of each individual in the cohort by calculating the node strength and eigenvector centrality. Both centrality measures, node strength and eigenvector centrality, were calculated on the same number of links (network density) across all individual networks. This was done to preserve

Node Strength The simplest measure of network centrality is degree centrality, which quantifies the number of connections a node has with other nodes in the network. In weighted networks – those of interest here – this measure is generalised to node strength (or weighted degree), which quantifies the strength of the functional connections of a node, rather than simply their count i.

Using the single-subject correlation matrix $\mathbf{r}^{(s)}_{t\in[t_m,t_m+\Delta t]}$, the node strength of node i for the s-th participant was computed within each sliding window t_m as the sum of its pairwise functional connections to all other nodes. Specifically, the node strength $\kappa^{(s)}_{t_m}(i)$ (see Eq. 2) quantifies the cumulative strength of functional interactions (defined by Eq. 1) between node i and the rest of the network during the sliding window $[t_m, t_m+\Delta t]$, with $m = 1,\ldots,N_{\text{win}}$.

$$\kappa^{(s)}_{t_m}(i) = \sum_{j=1,\, j\neq i}^{N_{ROI}} r^{(s)}_{t\in[t_m,t_m+\Delta t]}(i,j), \qquad i = 1,\ldots,N_{ROI}. \tag{2}$$

Eigenvector Centrality Eigenvector centrality is the centrality measure based on the assumption that connections to more influential nodes are more important than connections to less relevant nodes, while also taking into account the centrality of their neighbours. In simple terms, eigenvector centrality is the principal eigenvector of the network, which explains most of the variance in the data. Its principle is that links from important nodes (as measured by node strength) are worth more than links from unimportant nodes. All nodes start off equally, but as the computation progresses, nodes with more links gain importance. Their importance also influences the nodes to which they are connected to. After recomputing many times, the values stabilize and give the final eigenvector centrality values.

In general, an $M \times M$ non-singular, real-value matrix $\mathbf{B}$ can be decomposed into M independent eigenvectors $\vec{\psi}_m$ with associated eigenvalues λ_m, such that $\mathbf{B}\,\vec{\psi}_m = \lambda_m\,\vec{\psi}_m$ with $m = 1,\ldots,M$ (if the matrix is – as in our case — symmetric, then the eigenvalues are real-valued numbers). The eigenvector centrality network measure[2] is given by the eigenvector associated with the largest eigenvalue ($\max_m\{\lambda_m\} = \lambda_M > 0$). The elements of this eigenvector provide a global measure of the relative importance of each node in the network, taking into account all connections in the network, not just those directly linked to node i. Using the single-subject correlation matrix $\mathbf{r}^{(s)}_{t\in[t_0,t_0+\Delta t]}$, the eigenvector centrality for the s-th participant was calculated as follows:

$$e_{t_\Delta}(i) = \frac{1}{\lambda_{t_\Delta}} \sum_{j=1}^{N_{node}} \rho_{t_\Delta}(i,j)\, e(j)_{t_\Delta}, \tag{3}$$

where λ_{t_Δ} is a constant that denotes the largest eigenvalue of ρ_{t_Δ} and $e_{t_\Delta}(i)$ denotes the i-th coordinate of the corresponding principal eigenvector; that is, a centrality score $e_{t_\Delta}(i)$ for each node i in an undirected network that fulfils $\rho_{t_\Delta}\,\vec{e}_{t_\Delta} = \lambda_{t_\Delta}\vec{e}_{t_\Delta}$. Thus, the eigenvector centrality $e_{t_\Delta}(i)$ of a node i is given by the weighted sum of the values within the principal eigenvector of direct neighbours, $\rho_{t_\Delta}(i,j)\,e_{t_\Delta}(j)$, and scaled by the proportionality factor $\lambda_{t_\Delta}^{-1}$. Here, $\rho_{t_\Delta}(i,j)$ is an element of the correlation matrix representing the strength of the pair-wise interaction between nodes i and j during the sliding window $t_\Delta = t \in [t_m, t_m+\Delta t]$, defining a time-varying vector $\vec{e}_{t_\Delta}$, whose elements are the $e_{t_\Delta}(i)$.

Statistical Analysis

Differences within FN and dFN across the cohorts We analysed differences at the individual-link level across cohorts using the non-parametric Kruskal-Wallis test[68]. To generate confidence interval for the test, we created 100 independent cohort realisations – each realisation randomly selects total of 150 participants from AD, MCI, and HC study groups, i.e., 50 from each ones. The selection was done in a way that a 15 : 35 female-to-male ratio was preserved in each sample of 50 participants. In more details, a single test was performed on 150 pair-wise correlations/network links $r^{(s)}_{t\in[t_0,t_0+\Delta t]}(i,j)$, where $s = 1,\ldots,150$ from the three re-sampled cohorts. We conclude a difference in functional connectivity across cohorts if the averaged static or dynamic p-value is below 0.05. Post hoc analyses of pairwise group differences were performed using the built-in MATLAB function multcompare, which applies rank-based multiple-comparison procedures and uses Dunnett's test by default. This procedure reports p-values adjusted for multiple comparisons, thereby controlling for Type I errors (false positives).

Random Forest Classifier

A random forest classifier was employed to distinguish between individuals with AD, MCI and HC based on their fMRI time series. To train the classifier we used the entire time series of 197 time points, or windows of 20, 40 and 60 points, from 120 JBA regions. For the purpose of classification, a subset of these regions – selected based on prior relevance – was used as the feature of interest and input to the model. The classifier leveraged region-specific time series features to capture distinguishing patterns in functional activity associated with each group, enabling group differentiation. The selection of regions was decided by statistical analyses of dFC and sFC networks, with regions/nodes showing significant group differences included in the input for the RF model. After the selection of the nodes for analysis, we reshaped the time series in order to include every time point as a separate feature. We then added the labels based on AD, MCI or HC clinical groups and we trained a RF classifier using stratified 10-Fold Cross-Validation. The classifier averages the results of 100 decision trees.

Author Contribution

N.R. conducted analysis on the fMRI data, prepared figures, and drafted the initial methods and results sections. V.B. performed the RF analysis, with M.F. contributing the same RF analysis on the dataset. V.V. supervised the project, conceptualised the study, and wrote the final manuscript.

Funding Declaration

N.R and M.F were supported by RSAT (Grant No. DSR1058-100), V.B. was funded by DSR1085-100.

References

1. Sporns, O. *Networks of the Brain* (MIT press, 2010).
2. Fornito, A., Zalesky, A. & Bullmore, E. *Fundamentals of brain network analysis* (Academic Press, 2016).
3. Bijsterbosch, J. & Beckmann, C. *An introduction to resting state fMRI functional connectivity* (Oxford University Press, 2017).
4. Mattson, M. P. Apoptosis in neurodegenerative disorders. *Nat. reviews Mol. cell biology* **1**, 120–130 (2000).
5. Zecca, L., Youdim, M. B., Riederer, P., Connor, J. R. & Crichton, R. R. Iron, brain ageing and neurodegenerative disorders. *Nat. Rev. Neurosci.* **5**, 863–873 (2004).
6. Pievani, M., de Haan, W., Wu, T., Seeley, W. W. & Frisoni, G. B. Functional network disruption in the degenerative dementias. *The Lancet Neurol.* **10**, 829–843 (2011).
7. Stam, C. J. Modern network science of neurological disorders. *Nat. Rev. Neurosci.* **15**, 683–695 (2014).
8. Eguiluz, V. M., Chialvo, D. R., Cecchi, G. A., Baliki, M. & Apkarian, A. V. Scale-free brain functional networks. *Phys. review letters* **94**, 018102 (2005).
9. Damoiseaux, J. S. *et al.* Consistent resting-state networks across healthy subjects. *Proc. national academy sciences* **103**, 13848–13853 (2006).
10. Honey, C. J. *et al.* Predicting human resting-state functional connectivity from structural connectivity. *Proc. Natl. Acad. Sci.* **106**, 2035–2040 (2009).
11. Bullmore, E. & Sporns, O. Complex brain networks: graph theoretical analysis of structural and functional systems. *Nat. reviews neuroscience* **10**, 186–198 (2009).
12. Bullmore, E. & Sporns, O. The economy of brain network organization. *Nat. Rev. Neurosci.* **13**, 336–349 (2012).
13. Borne, L. *et al.* The interplay of age, gender and amyloid on brain and cognition in mid-life and older adults. *Sci. Reports* **14**, 1–15 (2024).
14. Stam, C., Jones, B., Nolte, G., Breakspear, M. & Scheltens, P. Small-world networks and functional connectivity in alzheimer's disease. *Cereb. cortex* **17**, 92–99 (2007).
15. Binnewijzend, M. A. *et al.* Brain network alterations in alzheimer's disease measured by eigenvector centrality in fmri are related to cognition and csf biomarkers. *Hum. brain mapping* **35**, 2383–2393 (2014).
16. Luo, X. *et al.* Intrinsic functional connectivity alterations in cognitively intact elderly apoe ε4 carriers measured by eigenvector centrality mapping are related to cognition and csf biomarkers: a preliminary study. *Brain imaging behavior* **11**, 1290–1301 (2017).
17. Dai, Z. *et al.* Disrupted structural and functional brain networks in alzheimer's disease. *Neurobiol. aging* **75**, 71–82 (2019).
18. Lei, B. *et al.* Longitudinal score prediction for alzheimer's disease based on ensemble correntropy and spatial–temporal constraint. *Brain imaging behavior* **13**, 126–137 (2019).
19. He, Y., Chen, Z. & Evans, A. Structural insights into aberrant topological patterns of large-scale cortical networks in alzheimer's disease. *J. Neurosci.* **28**, 4756–4766 (2008).
20. Stam, C. *et al.* Graph theoretical analysis of magnetoencephalographic functional connectivity in alzheimer's disease. *Brain* **132**, 213–224 (2009).
21. Delbeuck, X., Van der Linden, M. & Collette, F. Alzheimer'disease as a disconnection syndrome? *Neuropsychol. review* **13**, 79–92 (2003).

22. Zhang, D. *et al.* Multimodal classification of alzheimer's disease and mild cognitive impairment. *Neuroimage* **55**, 856–867 (2011).

23. Gilligan, T. M. *et al.* No relationship between fornix and cingulum degradation and within-network decreases in functional connectivity in prodromal alzheimer's disease. *PloS one* **14**, e0222977 (2019).

24. de Haan, W. *et al.* Disruption of functional brain networks in alzheimer's disease: what can we learn from graph spectral analysis of resting-state magnetoencephalography? *Brain connectivity* **2**, 45–55 (2012).

25. Heringa, S. M. *et al.* Multiple microbleeds are related to cerebral network disruptions in patients with early alzheimer's disease. *J. Alzheimer's Dis.* **38**, 211–221 (2014).

26. Tijms, B. M. *et al.* Single-subject grey matter graphs in alzheimer's disease. *PloS one* **8**, e58921 (2013).

27. Seo, E. H. *et al.* Whole-brain functional networks in cognitively normal, mild cognitive impairment, and alzheimer's disease. *PloS one* **8**, e53922 (2013).

28. Brier, M. R. *et al.* Functional connectivity and graph theory in preclinical alzheimer's disease. *Neurobiol. aging* **35**, 757–768 (2014).

29. Lo, C.-Y. *et al.* Diffusion tensor tractography reveals abnormal topological organization in structural cortical networks in alzheimer's disease. *J. Neurosci.* **30**, 16876–16885 (2010).

30. Yao, Z. *et al.* Abnormal cortical networks in mild cognitive impairment and alzheimer's disease. *PLoS computational biology* **6**, e1001006 (2010).

31. Reijmer, Y. D. *et al.* Disruption of cerebral networks and cognitive impairment in alzheimer disease. *Neurology* **80**, 1370–1377 (2013).

32. Liu, Z. *et al.* Altered topological patterns of brain networks in mild cognitive impairment and alzheimer's disease: a resting-state fmri study. *Psychiatry Res. Neuroimaging* **202**, 118–125 (2012).

33. Wang, D., Belden, A., Hanser, S. B., Geddes, M. R. & Loui, P. Resting-state connectivity of auditory and reward systems in alzheimer's disease and mild cognitive impairment. *Front. human neuroscience* **14**, 280 (2020).

34. Chen, G. *et al.* Modular reorganization of brain resting state networks and its independent validation in alzheimer's disease patients. *Front. human neuroscience* **7**, 456 (2013).

35. Contreras, J. A. *et al.* Resting state network modularity along the prodromal late onset alzheimer's disease continuum. *NeuroImage: Clin.* **22**, 101687 (2019).

36. Vuksanović, V., Staff, R. T., Ahearn, T., Murray, A. D. & Wischik, C. M. Cortical thickness and surface area networks in healthy aging, alzheimer's disease and behavioral variant fronto-temporal dementia. *Int. J. Neural Syst.* **29**, 1850055, DOI: 10.1142/S0129065718500557 (2019).

37. Greicius, M. D., Srivastava, G., Reiss, A. L. & Menon, V. Default-mode network activity distinguishes alzheimer's disease from healthy aging: evidence from functional mri. *Proc. Natl. Acad. Sci.* **101**, 4637–4642 (2004).

38. Petrella, J., Sheldon, F., Prince, S., Calhoun, V. & Doraiswamy, P. Default mode network connectivity in stable vs progressive mild cognitive impairment. *Neurology* **76**, 511–517 (2011).

39. Agosta, F. *et al.* Resting state fmri in alzheimer's disease: beyond the default mode network. *Neurobiol. aging* **33**, 1564–1578 (2012).

40. Dillen, K. N. *et al.* Functional disintegration of the default mode network in prodromal alzheimer's disease. *J. Alzheimer's disease* **59**, 169–187 (2017).

41. Vuksanović, V. & Hövel, P. Functional connectivity of distant cortical regions: role of remote synchronization and symmetry in interactions. *NeuroImage* **97**, 1–8 (2014).

42. Alderson, T. H., Bokde, A. L., Kelso, J. S., Maguire, L. & Coyle, D. Metastable neural dynamics underlies cognitive performance across multiple behavioural paradigms. *Hum. brain mapping* **41**, 3212–3234 (2020).

43. Filippi, M., Spinelli, E. G., Cividini, C. & Agosta, F. Resting state dynamic functional connectivity in neurodegenerative conditions: a review of magnetic resonance imaging findings. *Front. neuroscience* **13**, 657 (2019).

44. Moguilner, S. *et al.* Dynamic brain fluctuations outperform connectivity measures and mirror pathophysiological profiles across dementia subtypes: a multicenter study. *Neuroimage* **225**, 117522 (2021).

45. He, X. *et al.* Disrupted dynamic network reconfiguration of the language system in temporal lobe epilepsy. *Brain* **141**, 1375–1389 (2018).

46. Weber, S. *et al.* Dynamic functional connectivity patterns in schizophrenia and the relationship with hallucinations. *Front. psychiatry* **11**, 227 (2020).

47. Rabany, L. *et al.* Dynamic functional connectivity in schizophrenia and autism spectrum disorder: Convergence, divergence and classification. *NeuroImage: Clin.* **24**, 101966 (2019).

48. Rubido, N., Riedel, G. & Vuksanović, V. Genetic basis of anatomical asymmetry and aberrant dynamic functional networks in alzheimer's disease. *Brain Commun.* **6**, fcad320 (2024).

49. Córdova-Palomera, A. *et al.* Disrupted global metastability and static and dynamic brain connectivity across individuals in the alzheimer's disease continuum. *Sci. reports* **7**, 1–14 (2017).

50. Quevenco, F. C. *et al.* Memory performance-related dynamic brain connectivity indicates pathological burden and genetic risk for alzheimer's disease. *Alzheimer's research & therapy* **9**, 1–11 (2017).

51. Núñez, P. *et al.* Abnormal meta-state activation of dynamic brain networks across the alzheimer spectrum. *NeuroImage* **232**, 117898 (2021).

52. Sendi, M. S. *et al.* The link between static and dynamic brain functional network connectivity and genetic risk of alzheimer's disease. *bioRxiv* (2021).

53. Son, S.-J., Kim, J. & Park, H. Structural and functional connectional fingerprints in mild cognitive impairment and alzheimer's disease patients. *PloS one* **12**, e0173426 (2017).

54. Demirtaş, M. *et al.* A whole-brain computational modeling approach to explain the alterations in resting-state functional connectivity during progression of alzheimer's disease. *NeuroImage: Clin.* **16**, 343–354 (2017).

55. Du, Y., Fu, Z. & Calhoun, V. D. Classification and prediction of brain disorders using functional connectivity: promising but challenging. *Front. neuroscience* **12**, 525 (2018).

56. Zhang, H., Meng, C., Di, X., Wu, X. & Biswal, B. Static and dynamic functional connectome reveals reconfiguration profiles of whole-brain network across cognitive states. *Netw. Neurosci.* **7**, 1034–1050 (2023).

57. Gonzalez-Castillo, J. & Bandettini, P. A. Task-based dynamic functional connectivity: Recent findings and open questions. *Neuroimage* **180**, 526–533 (2018).

58. Wiesman, A. I. *et al.* Somatosensory dysfunction is masked by variable cognitive deficits across patients on the alzheimer's disease spectrum. *EBioMedicine* **73** (2021).

59. Assem, M., Shashidhara, S., Glasser, M. F. & Duncan, J. Basis of executive functions in fine-grained architecture of cortical and subcortical human brain networks. *Cereb. Cortex* **34**, bhad537 (2024).

60. Song, J. Amygdala activity and amygdala-hippocampus connectivity: metabolic diseases, dementia, and neuropsychiatric issues. *Biomed. & Pharmacother.* **162**, 114647 (2023).

61. Lorenzini, L. *et al.* Eigenvector centrality dynamics are related to alzheimer's disease pathological changes in non-demented individuals. *Brain communications* **5**, fcad088 (2023).

62. Laakso, M. *et al.* Volumes of hippocampus, amygdala and frontal lobes in the mri-based diagnosis of early alzheimer's disease: correlation with memory functions. *J. neural transmission-Parkinson's disease dementia section* **9**, 73–86 (1995).

63. Weiner, M. W. *et al.* The alzheimer's disease neuroimaging initiative 3: Continued innovation for clinical trial improvement. *Alzheimer's & Dementia* **13**, 561–571 (2017).

64. Amunts, K., Mohlberg, H., Bludau, S. & Zilles, K. Julich-brain: A 3d probabilistic atlas of the human brain's cytoarchitecture. *Science* **369**, 988–992 (2020).

65. Pearson, K. Vii. note on regression and inheritance in the case of two parents. *proceedings royal society Lond.* **58**, 240–242 (1895).

66. Leonardi, N. & Van De Ville, D. On spurious and real fluctuations of dynamic functional connectivity during rest. *Neuroimage* **104**, 430–436 (2015).

67. Zalesky, A. & Breakspear, M. Towards a statistical test for functional connectivity dynamics. *Neuroimage* **114**, 466–470 (2015).

68. Kruskal, W. H. & Wallis, W. A. Use of ranks in one-criterion variance analysis. *J. Am. statistical Assoc.* **47**, 583–621 (1952).

69. Woolrich, M. W., Ripley, B. D., Brady, M. & Smith, S. M. Temporal autocorrelation in univariate linear modeling of fmri data. *Neuroimage* **14**, 1370–1386 (2001).

70. Jenkinson, M., Bannister, P., Brady, M. & Smith, S. Improved optimization for the robust and accurate linear registration and motion correction of brain images. *Neuroimage* **17**, 825–841 (2002).

71. Smith, S. M. Fast robust automated brain extraction. *Hum. brain mapping* **17**, 143–155 (2002).

72. Jenkinson, M. & Smith, S. A global optimisation method for robust affine registration of brain images. *Med. image analysis* **5**, 143–156 (2001).

Supplementary Information

Data Analysis

Data Acquisition We select high-definition T1-weighted (T1w) images and resting-state fMRI (rs-fMRI) data from the Alzheimer's Disease Neuroimaging Initiative 3 (ADNI-3) protocol[63]. T1w images are acquired using 3 Tesla scanners (GE, Siemens, or Philips), with 2 time acceleration, sagittaly (left to right), and using 1 mm slices of 1 mm^2 pixels (Field-Of-View = $208 \times 240 \times 256mm$; Echo Time (TE) = min full echo $\sim 3.0ms$; Time following Inversion Pulse (TI) = $900.0ms$; Repetition Time (TR) = $2300.0ms$, which approximately account to a total scan time of 6:20 minutes). rs-fMRI follow ADNI-3's basic EPI-BOLD protocol, where participants have their eyes open and are scanned for (nearly) 10 minutes using the same two-time accelerated $3T$ scanners, following an even/odd interleaved axial-slicing (inferior to superior) of $3.4mm$ with $(3.4375mm)^2$ pixels (FOV = $220 \times 220 \times 163mm$; $P >> A$ phase encoding; TE = $30ms$; TR = $3000ms$). More details at ADNI's web-page.

Pre-processing Pipeline Data pre-processing is done by FMRIB's Expert Analysis Tool[69] (`FEAT`[1]), involving a high-pass filter (cut-off of at $100s$; $0.01Hz$), motion corrections (`MCFLIRT`)[70], inter-leaved slice-timing corrections (using Fourier-space signal's phase-shifting), non-brain removal (`BET`)[71], spatial smoothing (using a Gaussian kernel of full-width-half-maximum $5mm$), and intensity normalisation. Such pre-processing is applied to all participants alike, holding filtered rs-fMRI in each participant's native space and with their original resolution (minimising data manipulation). Quality control is carried by a visual assessment of FEAT's outputs, where 3 AD, 3 MCI, and 2 HC participants are discarded due to poor boundary-based registration (BBR) of rs-fMRI to T1w images. In addition, we excluded 31 subjects from the study whose motion-correction residuals were identified as outliers relative to the rest of the cohort. Subjects across all groups who exhibited excessive motion during fMRI preprocessing (6 in the AD group, 13 in the MCI group, and 12 in the HC group) were therefore removed from the analysis. Following quality control of the FEAT processing outputs, these subjects showed abnormally high voxel-wise synchrony across the entire brain, indicating that motion correction was insufficient to adequately compensate for head movement during fMRI acquisition. A list of the subjects can be found in the OFS repository folder of this project.

Brain Atlas Registration (Reverse Normalisation) Registration of the atlas (from MNI space) to each participant's rs-fMRI native space is done by FMRIB's Linear Image Registration Tool[70,72] (FLIRT). FLIRT transforms the $2mm$ resolution atlas in MNI space to the resolution of the filtered rs-fMRI ($3.4375 \times 3.4375 \times 3.4mm$) in native space orientation. The necessary matrix transformation for this registration is obtained from FEAT's rs-fMRI registration step. This step involves a BBR of the rs-fMRI to the participant's T1w high-resolution brain-extracted image, which we obtain by applying the `fsl_anat`[2] (default) pipeline, and a registration to the standard MNI152 brain. For the JBA regions' list see Table .

Harvard-Oxford Brain Atlas: dFN analysis on pair-wise groups

An independent cortical parcellation was done based on the H-OBA 48 regions. Results of the post hoc analysis of group-wise differences are shown in Fig. 9.

[1] URL: FSL's wiki on FEAT pre-processing
[2] URL: FSL's wiki on fsl_anat

Supplementary Table 1. Juelich Brain Atlas regions. The mid lines indicate border between grey and white matter regions.

Indices	Region
1/2	Anterior intra-parietal sulcus hIP1 L/R
3/4	Anterior intra-parietal sulcus hIP2 L/R
5/6	Anterior intra-parietal sulcus hIP3 L/R
7/8	Amygdala centromedial group L/R
9/10	Amygdala laterobasal group L/R
11/12	Amygdala superficial group L/R
13/14	Broca's area BA44 L/R
15/16	Broca's area BA45 L/R
17/18	Hippocampus cornu ammonis L/R
19/20	Hippocampus entorhinal cortex L/R
21/22	Hippocampus dentate gyrus L/R
23/24	Hippocampal-amygdaloid transition area L/R
25/26	Hippocampus subiculum L/R
27/28	Inferior parietal lobule PF L/R
29/30	Inferior parietal lobule PFcm L/R
31/32	Inferior parietal lobule PFm L/R
33/34	Inferior parietal lobule PFop L/R
35/36	Inferior parietal lobule PFt L/R
37/38	Inferior parietal lobule Pga L/R
39/40	Inferior parietal lobule PGp L/R
41/42	Primary auditory cortex TE1.0 L/R
43/44	Primary auditory cortex TE1.1 L/R
45/46	Primary auditory cortex TE1.2 L/R
47/48	Primary motor cortex BA4a L/R
49/50	Primary motor cortex BA4p L/R
51/52	Primary somatosensory cortex BA1 L/R
53/54	Primary somatosensory cortex BA2 L/R
55/56	Primary somatosensory cortex BA3a L/R
57/58	Primary somatosensory cortex BA3b L/R
59/60	Sec som cortex/Parietal operculum OP1 L/R
61/63	Secondary SC/OP2 L/R
63/64	Secondary SC/OP3 L/R
65/66	Secondary SC/OP4 L/R
67/68	Superior parietal lobule 5Ci L/R
69/70	Superior parietal lobule 5L L/R
71/72	Superior parietal lobule 5M L/R
73/74	Superior parietal lobule 7A L/R
75/76	Superior parietal lobule 7M L/R
77/78	Superior parietal lobule 7PC L/R
79/80	Superior parietal lobule 7P L/R
81/82	Visual cortex V1 BA17 L/R
83/84	Visual cortex V2 BA18 L/R
85/86	Visual cortex V3V L/R
87/88	Visual cortex V4 L/R
89/90	Visual cortex V5 L/R
91/92	Premotor cortex BA6 L/R
92/93	Acoustic radiation R/L
94	Callosal body
95/96	Cingulum R/L
97/98	Corticospinal tract R/L
99	Fornix
100/101	Inferior occipito-frontal fascicle RL
102/103	Lateral geniculate body R/L
104	Mamillary body
105/106	Medial geniculate body R/L
107/108	Optic radiation R/L
109/110	Superior longitudinal fascicle R/L
111/112	Superior occipito-frontal fascicle R/L
113/114	Uncinate fascicle R/L
115/116	Insula Id1 L/R
117/118	Insula Ig1 L/R
119/120	Insula Ig2 L/R

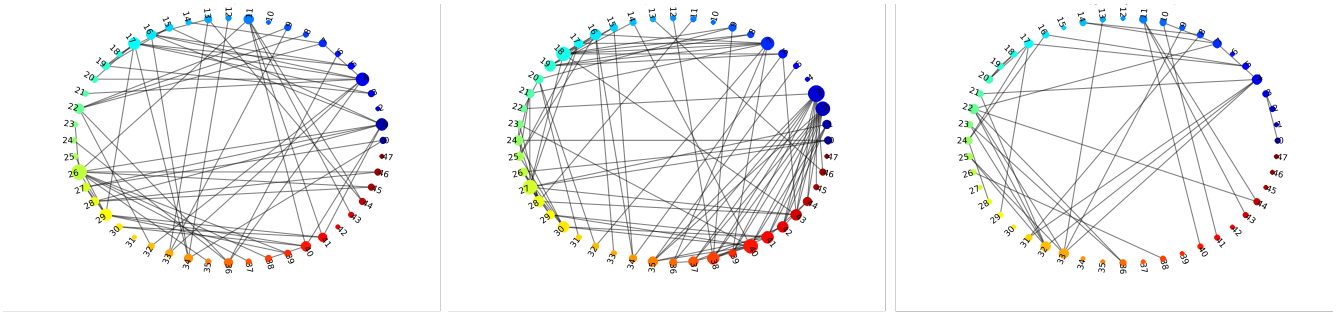

Figure 9. Significant differences at the link level between groups. Links (i.e., pair-wise correlations) are shown between nodes of the Harvard-Oxford Brain Atlas arranged on the circle when they passed a post-hoc analysis after the Kruskal-Walis tests applied to the each link's bootstrapped distributions (100 values for each test). Left: HC/AD; Center: HC/MCI; Right: MCI/AD. Colour coded are node lobar affiliations: Frontal (blue); parietal (green); temporal (yellow); occipital (red). Abbreviations: Alzheimer's disease (AD), mild cognitive impairment (MCI) and healthy controls (HC).